

Alternate Ascending/Descending Directional Navigation Approach for Imaging Magnetization Transfer Asymmetry

Sung-Hong Park* and Timothy Q. Duong†

A new method for imaging magnetization transfer (MT) asymmetry with no separate saturation pulse is proposed in this article. MT effects were generated from sequential two-dimensional balanced steady-state free precession imaging, where interslice MT asymmetry was separated from interslice blood flow and magnetic field inhomogeneity with alternate ascending/descending directional navigation (ALADDIN). Alternate ascending/descending directional navigation provided high-resolution multislice MT asymmetry images within a reasonable imaging time of ~3 min. MT asymmetry signals measured with alternate ascending/descending directional navigation were 1–2% of baseline signals ($N = 6$), in agreement with those from the conventional methods. About 70% of MT asymmetry signals were determined by the first prior slice. The frequency offset ranges in this study were >8 ppm from the water resonance frequency, implying that the MT effects were mostly associated with solid-like macromolecules. Potential methods to make alternate ascending/descending directional navigation feasible for imaging amide proton transfer (~3.5 ppm offset from the water resonance frequency) were discussed. *Magn Reson Med* 65:1702–1710, 2011. © 2010 Wiley-Liss, Inc.

Key words: magnetization transfer; magnetization transfer asymmetry; balanced steady-state free precession; alternate ascending/descending directional navigation; amide proton transfer; chemical exchange saturation transfer

Magnetization transfer (MT) effects (1) have been observed in MR imaging. MT effects that arise from interaction between solid-like macromolecules and bulk water exist in a wide range of frequency offsets from the water resonance frequency. The center of the spectral distribution of solid-like macromolecules in tissue is slightly lower than the center of the water resonance spectrum (2), hence these MT effects are not symmetric around the water resonance frequency (2–4). These conventional MT asymmetry effects were recently quantified using a modified two-pool MT model (3) and were demonstrated to reside in cervical spinal cords (5).

Distinct from the conventional MT effects, asymmetry in MT effects have been observed in frequency offsets < 8

ppm from the water resonance frequency, associated with amide protons of endogenous mobile proteins and peptides (4,6,7). The MT asymmetry imaging associated with amide proton transfer (APT) is one kind of chemical exchange saturation transfer techniques (8,9) and is sensitive to cellular pH (4,6,7). It has been shown to be useful for diagnosis of tumor (7,10–12) and stroke (4,13–15). In addition to APT, asymmetry in the conventional MT effects associated with solid-like macromolecules is also potentially useful for diagnosis of tumor (16). These factors emphasize necessity of reliable techniques for high-resolution multislice MT asymmetry imaging for clinical studies.

Imaging of MT asymmetry for clinical studies has not been easy because of its sensitivity to magnetic field inhomogeneity and difficulty in multislice acquisition. A few techniques have been proposed to correct magnetic field inhomogeneity in MT asymmetry imaging (4,7,12,17,18). These techniques require pixel by pixel correction of the offset frequency (4,7,17), establishment of a theoretical model in *in vivo* brains (18), or selection of an appropriate offset interval between three offset frequency points (12). Methods for multislice imaging of MT asymmetry also have been proposed in a few recent studies (13,19). In one of these techniques, the long MT saturation pulse was broken down into a series of short preparation pulses in multislice gradient echo sequence (19). One concern in the multislice imaging method is interslice MT effects, which have been commonly observed in general two-dimensional (2D) multislice imaging (20–23). These MT effects associated with multiple slices have been generally a confounding factor, but may be used as an alternative approach for imaging MT asymmetry.

In this article, a new method for imaging MT asymmetry with no saturation pulse is proposed. MT effects were generated from sequential 2D balanced steady-state free precession (bSSFP) imaging, where high interslice MT effects exist because of high flip angle and short pulse repetition time. For MT asymmetry, sequential 2D bSSFP slices were acquired by turns between acquisitions with MT effects at positive and negative frequency offsets. For the suppression of interslice blood flow, magnetic field inhomogeneity, and gradient imperfections, the positive and negative frequency offsets were generated by alternating ascending and descending slice orders and by alternating positive and negative slice-select gradients. This new MT asymmetry imaging technique, alternate ascending/descending directional navigation (ALADDIN), was tested at various scan conditions. ALADDIN MT asymmetry signals were measured in gray matter (GM) and white matter (WM) regions, and the results were compared with previously published values from the conventional methods.

Research Imaging Institute and Department of Radiology, University of Texas Health Science Center at San Antonio, San Antonio, Texas, USA.

Current affiliation for Dr. Park: Department of Radiology, School of Medicine, University of Pittsburgh, Pittsburgh, Pennsylvania, USA.

†This article was published online 30 July 2010. Timothy Q. Duong was subsequently acknowledged as a coauthor. This notice is included in the print and online versions to indicate that both have been corrected 19 May 2011.

*Correspondence to: Sung-Hong Park Ph.D., 200 Lothrop Street PUH-B864.2, Pittsburgh, PA 15213. E-mail: parks@upmc.edu

Received 22 March 2010; revised 24 May 2010; accepted 10 June 2010.

DOI 10.1002/mrm.22568

Published online 30 July 2010 in Wiley Online Library (wileyonlinelibrary.com).

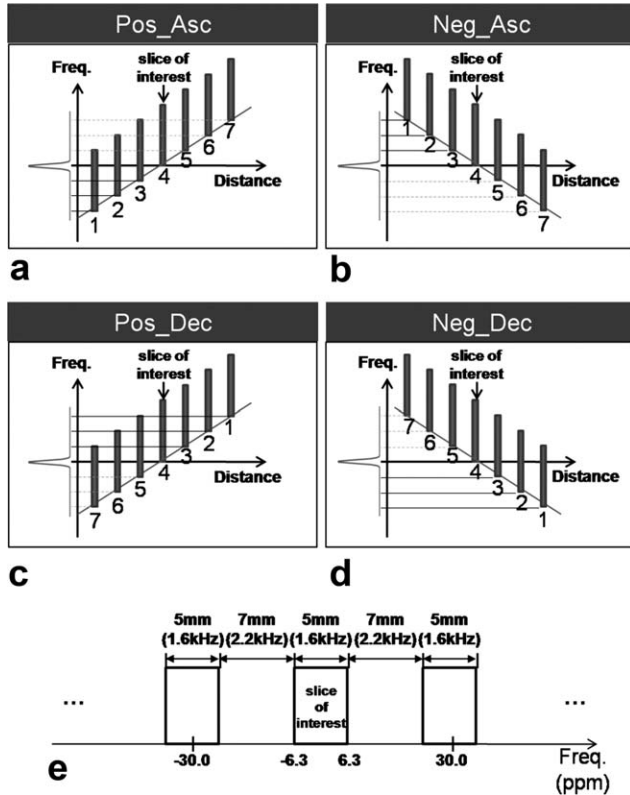


FIG. 1. Schematic diagram demonstrating magnetization transfer effects for ALADDIN. **a–d**: Frequency offsets of MT effects in the slice of interest (slice 4) from the surrounding six slices (1–3 and 5–7). The numbers under the slices represent the acquisition order. Because of the acquisition order, MT effects in the slice 4 are from the slices 1–3 (solid lines) but not from the slices 5–7 (dashed lines). Based on the diagram, acquisitions with the positive slice-select gradient and the ascending order (**a**, Pos_Asc) and with the negative slice-select gradient and the descending order (**d**, Neg_Des) cause MT effects in the slice 4 at negative frequency offsets, and acquisitions with the negative slice-select gradient and the ascending order (**b**, Neg_Asc) and with the positive slice-select gradient and the descending order (**c**, Pos_Des) cause MT effects in the slice 4 at positive frequency offsets. No separate saturation pulse exists in ALADDIN. **e**: Frequency offsets in parts per million (ppm) unit along with physical distances and frequencies in Hertz for the default gap value of 7 mm (140% of the thickness).

THEORY

The 2D multislice imaging is generally confounded by interslice MT (20–23) and blood flow effects (24). The goal of this study is to maximize interslice MT effects and separate them from interslice blood flow effects. Although conventional MT ratio imaging is useful for clinical studies and can be assessed with the ALADDIN approach, this study is focused on MT asymmetry imaging, which is potentially more useful for the diagnosis of diseases.

To get MT asymmetry, two sets of images need to be acquired: one with MT effects at positive frequency offsets and the other with those at negative frequency offsets from the water resonance frequency (3,4). In sequential 2D multislice imaging, the polarity of frequency offsets of interslice MT effects can be manipulated in two different ways: one with two different

acquisition orders, i.e., ascending and descending, and the other with two different slice-select gradient polarities, i.e., positive and negative, as shown in Fig. 1a–d. In Fig. 1a–d, the slice of interest (slice 4) would experience MT effects from the acquisition of the prior slices (slices 1–3). In terms of interslice blood flow, blood spins will be partially saturated when the acquisition order is in the same direction as the blood movement, whereas they will not be affected when the acquisition order is reversed. In the regions of magnetic field inhomogeneity, the radiofrequency (RF) pulse will excite a location slightly different between the positive and negative slice-select gradients. In terms of MT asymmetry, therefore, the ascending/descending approach is confounded by interslice blood flow and the positive/negative slice-select gradient approach by magnetic field inhomogeneity. Eventually, combination of the four datasets will compensate both the interslice blood flow and magnetic field inhomogeneity effects, as described later in this study.

In addition to the interslice MT and blood flow and magnetic field inhomogeneity, direct signal saturation from crosstalk between contiguous slices may also affect the ALADDIN signals. To avoid the interslice crosstalk, a relatively big gap (140% of slice thickness) was used in most studies in this article, based on an experimentally measured RF excitation profile described later.

MATERIALS AND METHODS

Data Acquisitions

All experiments in this study approved by the Institutional Review Board were performed on a 3-T whole-body scanner (Siemens Medical Solutions, Erlangen, Germany) with a 12-element head matrix coil for six normal volunteers. To get MT asymmetry images free of interslice blood flow, magnetic field inhomogeneity, and gradient imperfections, 2D bSSFP images were acquired in four different ways: two with positive slice-select gradient in sequentially ascending (Pos_Asc) and descending (Pos_Des) orders and the other two with negative slice-select gradient also in sequentially ascending (Neg_Asc) and descending (Neg_Des) orders (Fig. 1a–d). Note that the frequency offsets of MT effects are negative in Pos_Asc and Neg_Des and positive in Neg_Asc and Pos_Des (Fig. 1a–d). The four acquisitions were repeated for average. Default imaging parameters were as follows: pulse repetition time/echo time = 4/2 msec; flip angle = 50°; matrix size = 128 × 96; field of view = 240 × 180 mm²; thickness = 5 mm; gap = 7 mm (140% of thickness); number of slices = 15 (including dummy slices on each side); scan direction = axial; phase-encoding (PE) order = linear; PE direction = left–right; bandwidth and duration of excitation RF pulse = 1.6 kHz and 1 msec, respectively; dummy PE steps = 10; and scan time = ~3 min. These scan parameters were maintained for most ALADDIN acquisitions unless specified otherwise. For the investigation of the effects of number of PE steps on ALADDIN signals, three ALADDIN MT asymmetry datasets were acquired with phase oversampling = 0, 100, and 200% and corresponding total number of repetitions = 24, 12, and 8, respectively, which maintained the

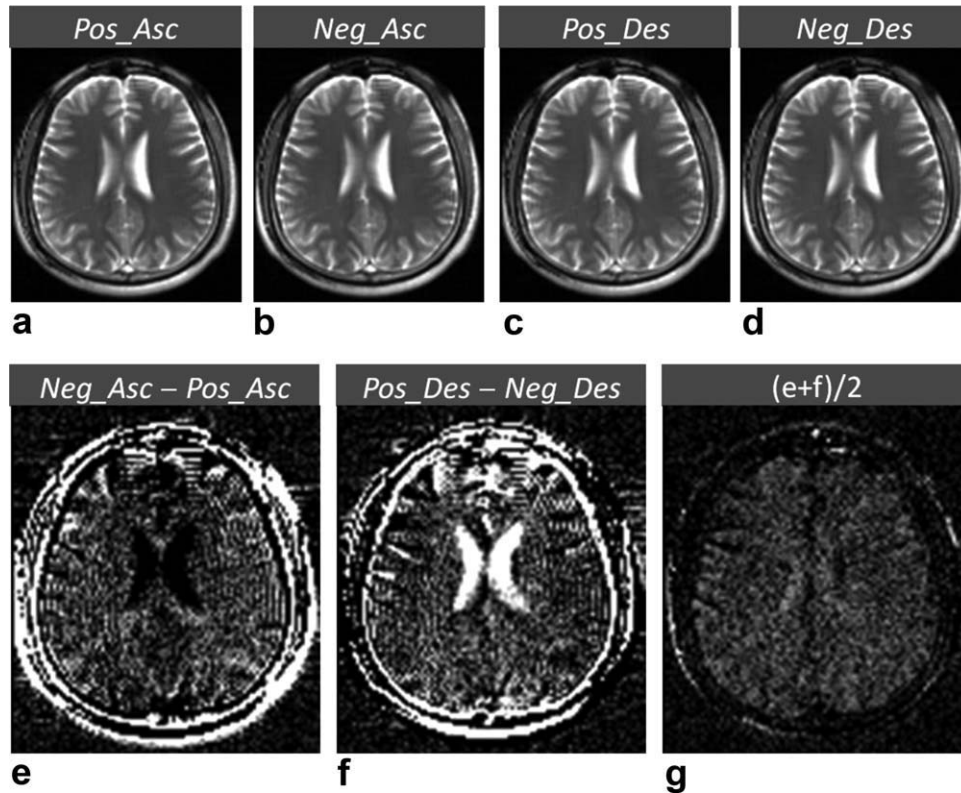


FIG. 2. Demonstration of effects of alternate acquisition orders and slice-select gradient polarities for ALADDIN. Data were acquired with phase oversampling = 100% from one representative subject. **a–d**: Baseline images acquired with ascending (a and b) and descending (c and d) orders and with positive (a and c) and negative (b and d) slice-select gradients. **e** and **f**: Subtraction images between ascending orders (e) and between descending orders (f) to suppress interslice blood flow effects. Subtraction polarity was decided such that images with MT effects at negative offsets (Pos_Asc, Neg_Des) were subtracted from images with MT effects at positive offsets (Neg_Asc, Pos_Des). The two subtraction images still showed artifactual signals due to magnetic field inhomogeneity and/or gradient imperfection. The artifactual signals were further compensated by averaging the two subtraction images (**g**). Images in **e–g** have the same intensity scale. The MT effects were mostly from frequency offsets of ± 30 ppm from the water resonance frequency.

same scan time and voxel size for the three datasets. Note that signal-to-noise ratio (SNR) of baseline images remained the same with phase oversampling, although number of repetitions hence number of averages decreased. This number of PE step-dependent study was performed for all the six subjects. Two more ALADDIN MT asymmetry datasets were acquired with number of slices of 9 and 3, and another two datasets with gap = 4 and 1 mm (80% and 20% of thickness). Finally, two additional MT asymmetry images were acquired along sagittal and coronal directions with number of slices = 19 to cover wider regions. A square field of view (240×240 mm²) was used for the sagittal scan. The scan time for the sagittal and coronal images was 4.6 and 3.6 min, respectively. These studies dependent on number of slices, gap, and scan direction were performed with phase oversampling = 0% (total number of repetition = 24) for three subjects and with phase oversampling = 100% (total number of repetition = 12) for the other three subjects.

The abovementioned gap-dependent studies were performed for two uniform phantoms with no MT effects: one with T_1 and T_2 of 110 and 75 msec, respectively, and the other with T_1 and T_2 of 4000 and 500 msec, respectively. RF excitation profile was measured by acquiring two consecutive axial and sagittal bSSFP

images with a higher in-plane resolution of 0.8×0.8 mm² using the phantom with long T_1 and T_2 .

Note that the default gap value (7 mm, 140% of thickness) generated MT asymmetry effects at the frequency offset of 30.0 ± 6.3 ppm (Fig. 1e) and the gap values of 4 and 1 mm those at the frequency offsets of 22.5 ± 6.3 ppm and 15.0 ± 6.3 ppm, respectively, from the first prior slice. These frequency offsets linearly increased as a function of distance between the slice of interest and a prior slice. For instance, MT effects in the slice of interest were generated at the frequency offsets of 60.0 ± 6.3 ppm and 90.0 ± 6.3 ppm from the second and third prior slices, respectively, for the default gap value.

Reconstruction

There were four different datasets of Pos_Asc, Neg_Asc, Pos_Des, and Neg_Des, which were repeatedly acquired for average in each ALADDIN acquisition (Fig. 2a–d). After each of the four datasets was averaged, images with MT effects at negative offsets were subtracted from images with MT effects at positive offsets, and the subtraction was performed between ascending acquisitions and between descending acquisitions to remove interslice blood flow effects, i.e., Neg_Asc – Pos_Asc (Fig.

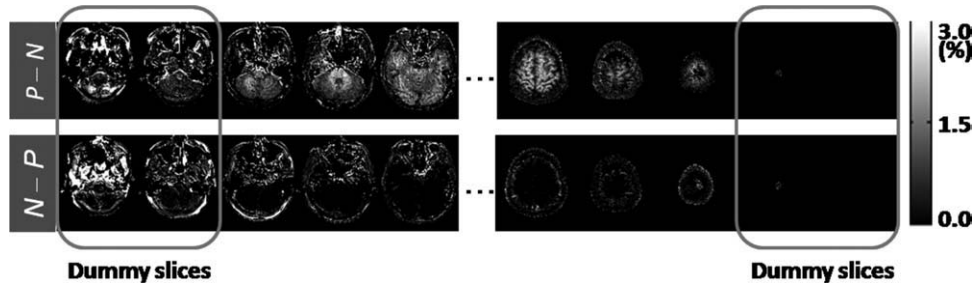


FIG. 3. Demonstration of transient MT effects in edge slices for ALADDIN. Top images are from subtraction of images with MT effects at negative offsets (N) from images with MT effects at positive offsets (P) (hence P-N), and bottom images are those with the subtraction polarity reversed (N-P). Data are displayed as percent signal changes from a subject different from Fig. 2. Signals in the 1-2 edge slices on each side of imaging group were not in the steady state because of transient MT and incomplete T_1 recovery effects. The total number of slices including dummy slices was 15 and the scan time was 3.0 min. The MT effects were mostly from frequency offsets of ± 30 ppm from the water resonance frequency.

2e) and Pos_Des - Neg_Des (Fig. 2f). The effects of magnetic field inhomogeneity and/or gradient imperfections were still observable in these subtraction images (Fig. 2e,f). These artifactual signals could be suppressed by averaging the two subtraction images of Neg_Asc - Pos_Asc and Pos_Des - Neg_Des (Fig. 2g). Finally, MT asymmetry images were displayed as percent signal change (PSC), i.e., average of the two subtraction images (Fig. 2g) divided by average of the baseline images (Fig. 2a-d) after appropriate thresholding. PSC is similar to the definition of the conventional MT asymmetry (4,7), except the facts that baseline signals with no MT effects are replaced with average baseline signals with MT effects in the denominator and that the subtraction polarity is opposite to the conventional definition (to make the signals positive). It should be noted that MT asymmetry signals in the previous literatures are negative when the frequency offset is >8 ppm from the water resonance frequency (3,4).

For the measurement of PSC and SNR, whole GM and WM regions and a noise region outside brain were manually segmented in the center slice of baseline images. PSC was measured from the abovementioned PSC images, and SNR was measured from the average of the two subtraction images (Fig. 2g).

RESULTS

ALADDIN with the four different acquisitions (Pos_Asc, Neg_Asc, Pos_Des, and Neg_Des) could suppress the effects of interslice blood flow, magnetic field inhomogeneity, and gradient imperfection, as demonstrated in Fig. 2. ALADDIN MT asymmetry images were mostly stable except for a few edge slices (Fig. 3), which were discarded as dummy slices. Visually, 1-2 dummy slices on each side were enough to ensure the steady state (Fig. 3). MT asymmetry signals in brain regions were observable in the PSC images reconstructed as described above (top in Fig. 3), but were not observable when the subtraction polarity was reversed (bottom in Fig. 3). This implies that the MT effects at negative offsets (Pos_Asc and Neg_Des, Fig. 1a,d) are slightly higher (baseline intensities decreased more) than the MT effects at positive offsets (Neg_Asc and Pos_Des; Fig. 1b,c), consistent with the observations from the previous studies (2-4).

Data from one representative subject acquired with phase oversampling = 0% are shown in Fig. 4. The axial MT asymmetry images (bottom row in Fig. 4) showed many hypointense spots and lines throughout the brain regions, which were not distinguishable in the corresponding baseline images (top row in Fig. 4). PSC values

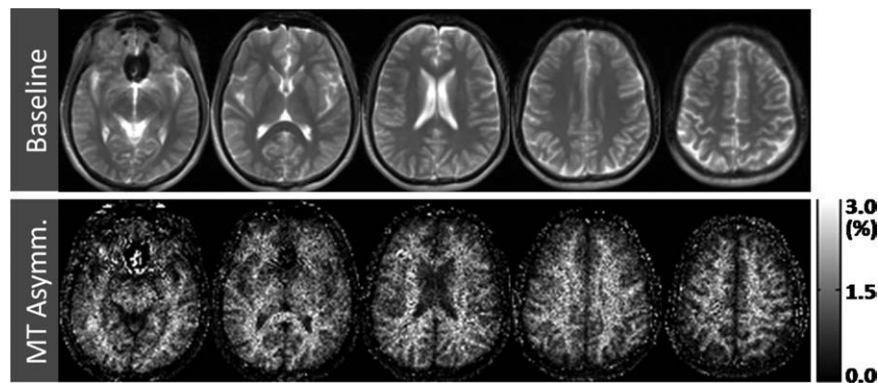


FIG. 4. One representative baseline images (top) and corresponding ALADDIN MT asymmetry images (bottom) acquired from a subject different from Figs. 2 and 3. Detailed structures are detectable following the cortical regions of gray matter and white matter in the MT asymmetry images (bottom). The total number of slices including dummy slices was 15 and the scan time was 3.0 min. The dark signals in the leftmost images are banding artifacts of balanced SSFP. The MT effects were mostly from frequency offsets of ± 30 ppm from the water resonance frequency.

Table 1
Percent Signal Change (PSC) and Signal-to-Noise Ratio (SNR) Measured over Gray Matter (GM) and White Matter (WM) Regions in ALADDIN MT Asymmetry Images

| Common parameters | Differences | PSC (%) | | SNR | |
|---|-------------|-----------|-----------------------|-----------|-----------|
| | | GM | WM | GM | WM |
| Slice 15, gap 140% ($N = 6$) | PH_OS 0% | 1.1 ± 0.1 | 1.8 ± 0.2 | 4.9 ± 0.9 | 6.4 ± 1.0 |
| | PH_OS 100% | 1.0 ± 0.1 | 1.4 ± 0.1 | 3.1 ± 0.4 | 3.4 ± 0.4 |
| | PH_OS 200% | 0.8 ± 0.1 | 0.9 ± 0.1 | 2.1 ± 0.3 | 1.8 ± 0.1 |
| Gap 140%, PH_OS 0% ($N = 3$) | Slice 15 | 1.0 ± 0.0 | 1.8 ± 0.0 | 4.5 ± 0.2 | 6.1 ± 0.5 |
| | Slice 9 | 1.0 ± 0.1 | 1.8 ± 0.1 | 4.3 ± 0.5 | 5.7 ± 0.2 |
| | Slice 3 | 0.6 ± 0.1 | 1.2 ± 0.0 | 2.5 ± 0.1 | 4.0 ± 0.5 |
| Gap 140%, PH_OS 100% ($N = 3$) | Slice 15 | 1.0 ± 0.1 | 1.4 ± 0.1 | 3.4 ± 0.2 | 3.6 ± 0.1 |
| | Slice 9 | 1.0 ± 0.1 | 1.4 ± 0.1 | 3.6 ± 0.4 | 3.6 ± 0.3 |
| | Slice 3 | 0.5 ± 0.1 | 1.0 ± 0.1 | 1.9 ± 0.5 | 2.6 ± 0.5 |
| Slice 15, PH_OS 0% ($N = 3$) | Gap 80% | 1.3 ± 0.0 | 2.2 ± 0.1 | 5.0 ± 0.2 | 6.3 ± 0.3 |
| | Gap 20% | 1.4 ± 0.1 | 2.2 ± 0.1 | 4.5 ± 0.4 | 5.4 ± 0.3 |
| Slice 15, PH_OS 100% ($N = 3$) | Gap 80% | 1.2 ± 0.1 | 1.5 ± 0.1 | 4.1 ± 0.8 | 3.8 ± 0.4 |
| | Gap 20% | 0.9 ± 0.1 | 1.2 ± 0.2 | 2.8 ± 0.2 | 2.8 ± 0.3 |
| Pulsed saturation methods at 30-ppm offset (3) | Pulsed 1 | N/A | 2.6 ± 0.9 (1.7 ± 0.6) | N/A | N/A |
| | Pulsed 2 | N/A | 1.7 ± 2.5 (1.3 ± 1.9) | N/A | N/A |

PH_OS represents phase oversampling. Number of averages was 12, 6, and 4 when phase oversampling = 0, 100, and 200%, respectively. All the values are measured from the center slice of each imaging group and are given as mean ± standard deviation across subjects. The values from the literature (3) are those after conversion into PSC, and the values inside the parenthesis are the original MT asymmetry values before the conversion. The "Pulsed 1" was from a pulse train of 15 Gaussian pulses (length 115 msec, interval 85 msec, flip angle 4135°, total duration 3 sec) with the equivalent power (compared with the block shape) of 2.3 μ T, and the "Pulsed 2" was from 24.5-msec nonselective five-lobed sinc-gauss MT pulse with peak amplitude of 10.5 μ T (3).

of ALADDIN MT asymmetry signals were roughly in the similar range to those from the conventional pulsed MT preparation methods (3) (Table 1). Note that the RF power used in this study corresponds to the continuous wave with 0.8 μ T, which is lower than the power used in the conventional methods (2.3 μ T) (3).

Lower phase oversampling rates (i.e., smaller number of PE steps) resulted in better MT asymmetry image qualities (Fig. 5a) because of higher PSC values as well as higher SNR (Table 1). The result implies that the optimal number of PE steps may be even smaller than the PE steps of phase oversampling = 0% (96 PE steps) with a given scan time of ~3 min. Generally, both PSC and SNR values in WM were higher than those in GM, but the difference between GM and WM decreased with phase oversampling (Table 1).

In the number of slice-dependent studies, MT asymmetry signals in the center slice were almost the same between the number of slices of 15 and 9, but were reduced to 70% of the signals when number of slice was 3 (Fig. 5b and Table 1). There was no significant difference between phase oversampling of 0% and 100% in response to changes in the number of slices (Table 1). These results imply that ~70% of ALADDIN MT asymmetry signals in a slice are ascribed to the first prior slice regardless of phase oversampling.

MT asymmetry signals generally increased when gap was reduced from 140% to 80% of the thickness but remained the same or even decreased when gap was further reduced to 20% of the thickness (Table 1). Images from one representative subject and the two uniform phantoms with phase oversampling = 100% are shown in Fig. 6a. When gap was 20% of the thickness, the number and contrast of hypointense structures (spots and lines) increased (top row in Fig. 6a), and these hypointense structures presumably

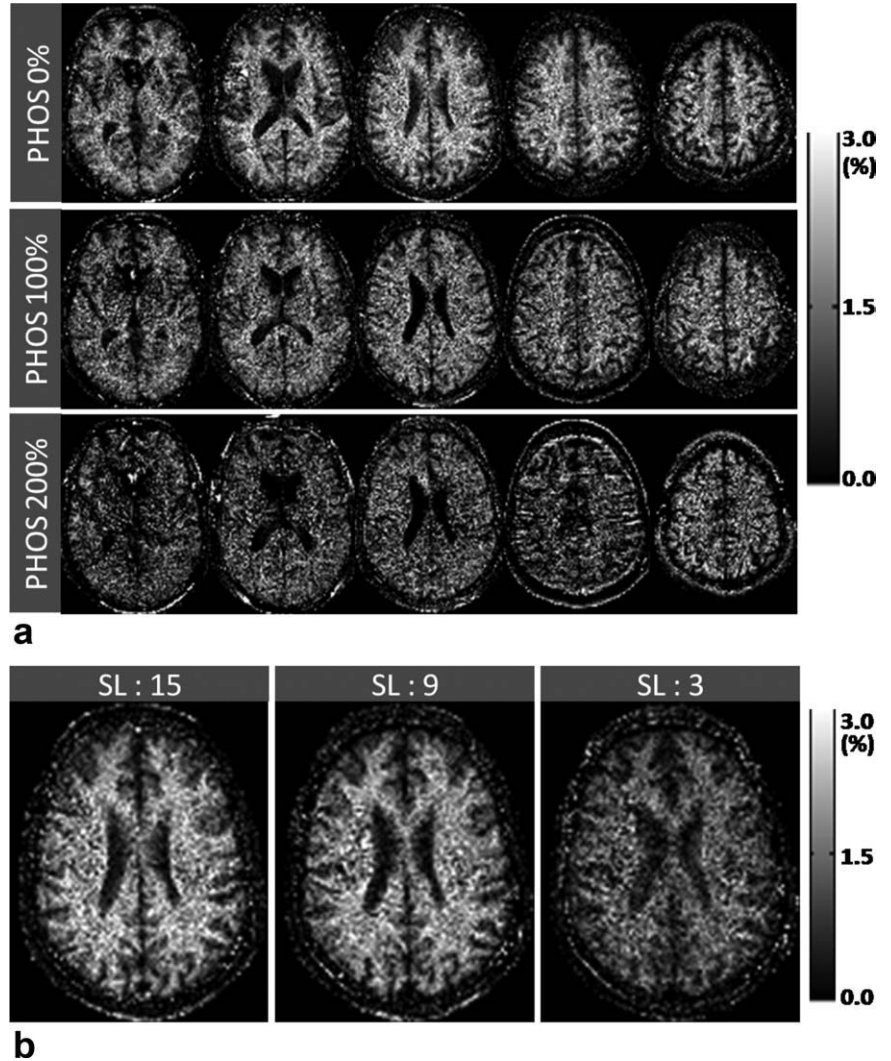
from susceptibility effects of veins or iron deposits were bright when subtraction polarity was reversed. PSC of MT asymmetry from the phantom with short T_1 and T_2 (phantom 1) was 0.0% ± 0.1% for all the three gap values and that from the phantom with long T_1 and T_2 (phantom 2) was 0.1% ± 0.4%, 0.1% ± 0.2%, and 0.1% ± 0.2% when gap was 140%, 80%, and 20%, respectively, of the thickness (bottom row in Fig. 6a). The phantom results imply that crosstalk effects may not be the main source of the characteristics of the gap-dependent in vivo ALADDIN signals (top row in Fig. 6a). However, the experimentally measured RF excitation profile showed that only gap of 140% of the thickness was free of crosstalk effects (Fig. 6b). Therefore, all the studies in this article except the gap-dependent study were performed with gap of 140% of the thickness.

In sagittal and coronal ALADDIN MT asymmetry images (Fig. 7), WM signals were higher than GM signals, consistent with axial MT asymmetry images. All the sagittal and coronal MT asymmetry signals were observable in images reconstructed in the method described above (Fig. 7), but were not observable when subtraction polarity was reversed, also consistent with the axial images. MT asymmetry in GM and WM of cerebellum was also clearly detectable in the sagittal and coronal MT asymmetry images (Fig. 7).

DISCUSSION

In this article, it is demonstrated that ALADDIN provides images of MT asymmetry with no separate saturation pulse. The excitation RF pulse for imaging a slice works simultaneously as MT saturation for the following slices in ALADDIN. ALADDIN is well suited for high-

FIG. 5. Number of phase-encoding (PE) step-dependent and number of slice-dependent experiments for ALADDIN from a subject different from Figs. 2–4. **a**: Number of PE step-dependent experiments. ALADDIN MT asymmetry images were acquired with phase oversampling = 0, 100, and 200% and corresponding number of PE steps of 96, 192, and 288, respectively (top, middle, and bottom rows, respectively). The scan time was almost the same (3 min). **b**: Number of slice-dependent experiments. Data were acquired with phase oversampling = 0%. “SL” represents the total number of slices. The displayed images are the center slice of each imaging group. The MT effects were mostly from frequency offsets of ± 30 ppm from the water resonance frequency.



resolution multislice MT asymmetry imaging free of magnetic field inhomogeneity, which has not been easily achieved in previous methods. Effects of blood flow, magnetic field inhomogeneity, and gradient imperfections could be mostly compensated by combining four different types of datasets acquired with ascending and descending slice orders and with positive and negative slice-select gradients (Fig. 2).

Blood flow signals in GM are generally higher than those in WM, but the trend was opposite in MT asymmetry images (Figs. 4–7), consistent with the results from MT ratio imaging (25,26). Also, blood flow direction is expected to be from brain center to edges in case of sagittal and coronal scans based on vascular anatomy, whereas there was no change in signal polarity in the sagittal and coronal MT asymmetry images throughout the brain regions (Fig. 7). According to the RF excitation profile, interslice crosstalk would not contribute to the ALADDIN signals when gap was 140% of the thickness (Fig. 6b). These results imply that MT asymmetry signals in this article are well separated from the other sources, i.e., interslice blood flow and crosstalk effects.

As ALADDIN is feasible for MT asymmetry, it would also be feasible for MT ratio imaging, which has been

also useful for clinical studies (27,28). By additionally acquiring ALADDIN images free of MT effects with a long interslice delay time, the MT ratio would be measurable and thus the MT asymmetry would be also measurable in the conventional definition (4,7).

As ascending and descending slice orders were alternated in successive acquisitions in this study, transient MT effects and incomplete T_1 recovery in edge slices would be mostly determined by the slice order rather than the slice-select gradient polarity. Subtraction in MT asymmetry was performed either between the two ascending acquisitions or between the two descending acquisitions (Fig. 2), hence the transient MT effects and incomplete T_1 recovery in edge slices were relatively well suppressed by the subtraction. The relatively small number (1 or 2) of dummy slices (Fig. 3) might be attributed to this condition. The number of slice-dependent studies demonstrated the significant contributions ($\sim 70\%$) of the first prior slice to ALADDIN signals regardless of phase oversampling. Therefore, about two dummy slices were enough to ensure the steady state of MT asymmetry signals.

According to the gap-dependent study, the sensitivity of ALADDIN can be enhanced by reducing the gap down

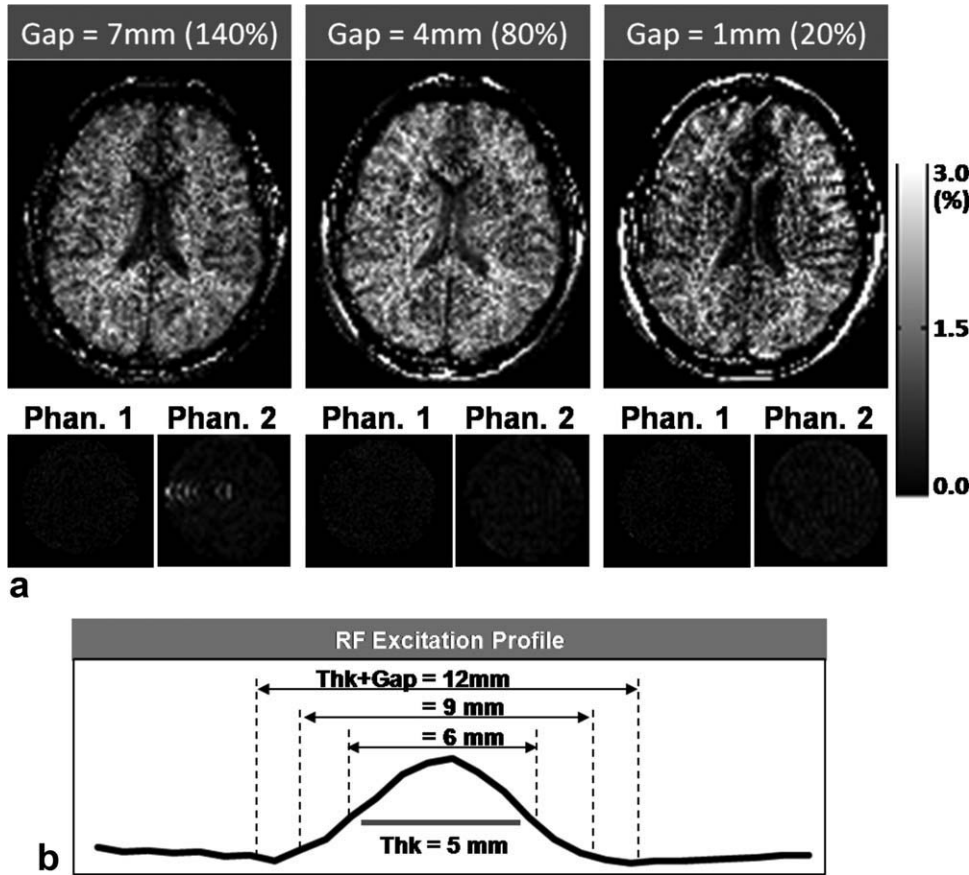


FIG. 6. Gap-dependent experiments and RF excitation profile for ALADDIN. **a**: Gap-dependent experiments. The images are from a subject different from Figs. 2–5 (top row) and from two uniform phantoms (bottom row). T_1 and T_2 values of one phantom (phantom 1) were 110 and 75 msec, respectively, and those of the other phantom (phantom 2) were 4000 and 500 msec, respectively. Data were acquired with phase oversampling = 100%. The MT effects were mostly from frequency offsets of ± 30 , ± 22.5 , and ± 15 ppm from the water resonance frequency for the gap value of 140% (left), 80% (middle), and 20% (right), respectively. **b**: Experimentally measured RF excitation profile. The excitation thickness was 5 mm (gray bar), and the vertical broken lines represent the boundaries of a slice in consideration of the three gap values.

to 80% of the thickness. This may be achievable without crosstalk effects by improving the excitation profile of the RF pulse with a special method such as Shinnar-Le

Roux algorithm (29). In this study, the gap was set to a high value (140% of the thickness) to avoid crosstalk artifacts. With a big interslice gap value (e.g. 100–140%

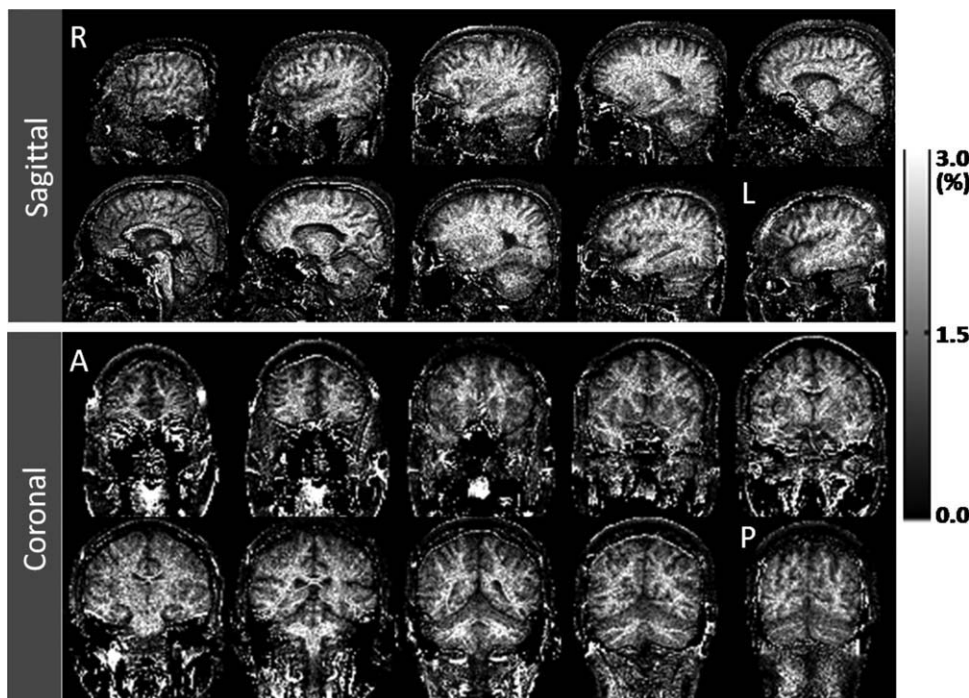


FIG. 7. Sagittal and coronal ALADDIN MT asymmetry images acquired with phase oversampling = 0% from the same subject shown in Fig. 2 (sagittal, top) and a subject different from Figs. 2–6 (coronal, bottom). The total number of slices including the dummy slices on each side was 19. The scan time for sagittal and coronal scans was 4.6 and 3.6 min, respectively. The MT effects were mostly from frequency offset of ± 30 ppm from the water resonance frequency. Images are displayed from right (R) to left (L) for sagittal scans (top) and from anterior (A) to posterior (P) for coronal scans (bottom).

of the thickness), still whole brain MT asymmetry imaging will be possible in ALADDIN with a conventional gap value (e.g., 0–20% of the thickness) by acquiring two datasets in a location interleaved to each other.

The MT effects hence asymmetry effects in this study are mostly from solid-like macromolecules in the frequency offset range >8 ppm from the water resonance frequency. One potential method to make ALADDIN feasible for APT imaging (~3.5 ppm from the water resonance frequency) is to use a long excitation RF pulse. If we increase the RF duration from 1.0 to 8.6 msec, the frequency offset from the first prior slice will be reduced from 30 ppm to 3.5 ppm with the default gap value (140% of the thickness). There are two potential problems associated with this approach: one is long pulse repetition time for bSSFP (from 4 to 11.6 msec) hence increased banding artifacts and the other is RF duty cycle limit. The interslice frequency offsets can be reduced by improving the RF excitation profile hence by reducing the interslice gap (e.g., 80% of thickness) as mentioned above, which enables to reduce the RF duration for APT imaging (e.g., 6.5 msec). High-field MR systems such as 7 T (30) are advantageous for APT imaging with ALADDIN in that the frequency offset of ~3.5 ppm can be achieved with a much shorter RF duration (e.g., 2.8 msec). As MT asymmetry signals in ALADDIN are from multiple prior slices, there will be ~30% contaminations from the second and third prior slices (~7 and ~10.5 ppm, respectively), although the frequency offset of the first prior slice can be adjusted to ~3.5 ppm. It should be noted that polarity of MT asymmetry signals at the frequency offset of ~3.5 ppm would be opposite to that at the frequency offsets >8 ppm (4).

The specific absorption rate in ALADDIN is expected to be lower than the conventional continuous or pulsed saturation methods (3,31) because of the absence of the RF power-demanding MT saturation part. The bSSFP is one of the most efficient sequences for ALADDIN MT asymmetry, because of high SNR of baseline images and high interslice MT saturation effects. Further studies are necessary to optimize scan protocols, quantitatively analyze the interslice MT effects (23), adjust frequency offsets of interslice MT effects to be ~3.5 ppm for APT imaging, compare ALADDIN with conventional continuous and/or pulsed wave methods, plot an *Z*-spectrum with ALADDIN, and apply ALADDIN to clinical studies.

CONCLUSIONS

ALADDIN provided high-resolution multislice MT asymmetry images with no separate spin preparation. Experimental results in this study supported that ALADDIN enabled good separation of interslice MT asymmetry signals from those associated with interslice blood flow and magnetic field inhomogeneity effects. ALADDIN MT asymmetry images showed some new structures that were not detectable in the corresponding baseline images. Characteristics of ALADDIN MT asymmetry signals were generally in agreement with those from the previous studies. Further studies are necessary for opti-

mization of ALADDIN and its applications to APT imaging and clinical studies.

REFERENCES

1. Wolff SD, Balaban RS. Magnetization transfer contrast (MTC) and tissue water proton relaxation in vivo. *Magn Reson Med* 1989;10:135–144.
2. Pekar J, Jezzard P, Roberts DA, Leigh JS, Jr, Frank JA, McLaughlin AC. Perfusion imaging with compensation for asymmetric magnetization transfer effects. *Magn Reson Med* 1996;35:70–79.
3. Hua J, Jones CK, Blakeley J, Smith SA, van Zijl PC, Zhou J. Quantitative description of the asymmetry in magnetization transfer effects around the water resonance in the human brain. *Magn Reson Med* 2007;58:786–793.
4. Zhou J, Payen JF, Wilson DA, Traystman RJ, van Zijl PC. Using the amide proton signals of intracellular proteins and peptides to detect pH effects in MRI. *Nat Med* 2003;9:1085–1090.
5. Ng MC, Hua J, Hu Y, Luk KD, Lam EY. Magnetization transfer (MT) asymmetry around the water resonance in human cervical spinal cord. *J Magn Reson Imaging* 2009;29:523–528.
6. van Zijl PC, Zhou J, Mori N, Payen JF, Wilson D, Mori S. Mechanism of magnetization transfer during on-resonance water saturation. A new approach to detect mobile proteins, peptides, and lipids. *Magn Reson Med* 2003;49:440–449.
7. Zhou J, Lal B, Wilson DA, Lartera J, van Zijl PC. Amide proton transfer (APT) contrast for imaging of brain tumors. *Magn Reson Med* 2003;50:1120–1126.
8. Ward KM, Aletras AH, Balaban RS. A new class of contrast agents for MRI based on proton chemical exchange dependent saturation transfer (CEST). *J Magn Reson* 2000;143:79–87.
9. Ward KM, Balaban RS. Determination of pH using water protons and chemical exchange dependent saturation transfer (CEST). *Magn Reson Med* 2000;44:799–802.
10. Jones CK, Schlosser MJ, van Zijl PC, Pomper MG, Golay X, Zhou J. Amide proton transfer imaging of human brain tumors at 3T. *Magn Reson Med* 2006;56:585–592.
11. Salhotra A, Lal B, Lartera J, Sun PZ, van Zijl PC, Zhou J. Amide proton transfer imaging of 9L gliosarcoma and human glioblastoma xenografts. *NMR Biomed* 2008;21:489–497.
12. Zhou J, Blakeley JO, Hua J, Kim M, Lartera J, Pomper MG, van Zijl PC. Practical data acquisition method for human brain tumor amide proton transfer (APT) imaging. *Magn Reson Med* 2008;60:842–849.
13. Sun PZ, Murata Y, Lu J, Wang X, Lo EH, Sorensen AG. Relaxation-compensated fast multislice amide proton transfer (APT) imaging of acute ischemic stroke. *Magn Reson Med* 2008;59:1175–1182.
14. Sun PZ, Zhou J, Huang J, van Zijl P. Simplified quantitative description of amide proton transfer (APT) imaging during acute ischemia. *Magn Reson Med* 2007;57:405–410.
15. Jokivarsi KT, Hiltunen Y, Tuunanen PI, Kauppinen RA, Grohn OH. Correlating tissue outcome with quantitative multiparametric MRI of acute cerebral ischemia in rats. *J Cereb Blood Flow Metab* 2010;30:415–427.
16. Hua J, van Zijl P, Sun PZ, Zhou J. Quantitative description of magnetization transfer (MT) asymmetry in experimental brain tumors. *Proc Int Soc Mag Reson Med* 2007;16:882.
17. Kim M, Gillen J, Landman BA, Zhou J, van Zijl PC. Water saturation shift referencing (WASSR) for chemical exchange saturation transfer (CEST) experiments. *Magn Reson Med* 2009;61:1441–1450.
18. Sun PZ, Farrar CT, Sorensen AG. Correction for artifacts induced by B(0) and B(1) field inhomogeneities in pH-sensitive chemical exchange saturation transfer (CEST) imaging. *Magn Reson Med* 2007;58:1207–1215.
19. Dixon WT, Hancu I, Ratnakar SJ, Sherry AD, Lenkinski RE, Alsop DC. A multislice gradient echo pulse sequence for CEST imaging. *Magn Reson Med* 2010;63:253–256.
20. Dixon WT, Engels H, Castillo M, Sardashti M. Incidental magnetization transfer contrast in standard multislice imaging. *Magn Reson Imaging* 1990;8:417–422.
21. Melki PS, Mulkern RV. Magnetization transfer effects in multislice RARE sequences. *Magn Reson Med* 1992;24:189–195.
22. Santyr GE. Magnetization transfer effects in multislice MR imaging. *Magn Reson Imaging* 1993;11:521–532.
23. Weigel M, Helms G, Hennig J. Investigation and modeling of magnetization transfer effects in two-dimensional multislice turbo spin echo

- sequences with low constant or variable flip angles at 3 T. *Magn Reson Med* 2010;63:230–234.
24. Williams DM, Meyer CR, Schreiner RJ. Flow effects in multislice, spin-echo magnetic resonance imaging. Model, experimental verification, and clinical examples. *Invest Radiol* 1987;22:642–650.
 25. Finelli DA, Reed DR. Flip angle dependence of experimentally determined T1sat and apparent magnetization transfer rate constants. *J Magn Reson Imaging* 1998;8:548–553.
 26. Bieri O, Scheffler K. On the origin of apparent low tissue signals in balanced SSFP. *Magn Reson Med* 2006;56:1067–1074.
 27. Miller DH, Grossman RI, Reingold SC, McFarland HF. The role of magnetic resonance techniques in understanding and managing multiple sclerosis. *Brain* 1998;121 (pt 1):3–24.
 28. Papanikolaou N, Ghiatas A, Kattamis A, Ladis C, Kritikos N, Kattamis C. Non-invasive myocardial iron assessment in thalassaemic patients. T2 relaxometry and magnetization transfer ratio measurements. *Acta Radiol* 2000;41:348–351.
 29. Pauly J, Roux PL, Nishimura D, Macovski A. Parameter relations for the Shinnar-Le Roux selective excitation pulse design algorithm. *IEEE Trans Med Imaging* 1991;10:53–65.
 30. Mougin OE, Coxon RC, Pitiot A, Gowland PA. Magnetization transfer phenomenon in the human brain at 7 T. *Neuroimage* 2010;49:272–281.
 31. Sun PZ, Benner T, Kumar A, Sorensen AG. Investigation of optimizing and translating pH-sensitive pulsed-chemical exchange saturation transfer (CEST) imaging to a 3T clinical scanner. *Magn Reson Med* 2008;60:834–841.